Isomorphic property of sheared three-dimensional Yukawa liquidlike fluids

Dong Huang and Yan Feng [*]
Institute of Plasma Physics and Technology, Jiangsu Key Laboratory of Frontier Material Physics and Devices, School of Physical Science and Technology, Soochow University, Suzhou 215006, China

(Received 29 July 2026; accepted 27 August 2026; published 11 September 2026)

The isomorphic property of strongly coupled three-dimensional (3D) Yukawa liquidlike fluids under steady shear is systematically investigated using nonequilibrium molecular dynamical simulations. It is discovered that, as the shear rate increases substantially, the shear viscosity η and the radial distribution function $g(r)$ both exhibit excellent isomorphic scaling properties. The isomorphic scaling of shear viscosity is attributed to the dominant role of neighboring particles, whose averaged local configuration of $g(r)$ is invariant, even though 3D Yukawa fluids are continuously deformed and rearranged by the applied shear. Furthermore, it is found that the Stokes-Einstein relation is violated at higher shear rates because the diffusion coefficient D is directional dependent and sensitive to the applied shear, i.e., not an isomorph invariant anymore.

DOI: 10.1103/md4x-9k3g

I. INTRODUCTION

The isomorph theory reveals invariance of various physical quantities expressed in properly reduced units in some liquids [1–3]. These liquids are termed the Roskilde-simple or R-simple liquids [3,4], which include atomic/molecular model liquids [5–7], generalized Lennard-Jones liquids [8,9], and Yukawa systems [10,11]. These R-simple liquids exhibit strong correlations between configurational virial and potential-energy fluctuations [12–14], resulting in isomorphs or isomorphic curves, along which reduced structure, dynamics, excess entropy, and selected thermodynamic quantities are approximately invariant [15,16]. The previous investigations demonstrate that various physical procedures under different conditions exhibit typical features of isomorphs, such as melting [17,18], freezing [17], transports [19–22], and relaxations [23].

Although the isomorph theory was originally developed for equilibrium systems [1–3], it has been demonstrated to be powerful to characterize not only equilibrium [10–14] and near-equilibrium systems [23,24], but also those far from thermal equilibrium [25–28], such as nonlinear steady flows [25,26] and active matter [27,28]. To study the momentum transport in liquids, it is a common practice to apply a steady shear from boundaries, so that the studied liquid is driven far from equilibrium, resulting in a flow velocity gradient $\dot{\gamma}$ [29–31]. Due to the applied steady shear, the time scale of externally imposed shear $\dot{\gamma}^{-1}$ competes with the intrinsic relaxation time of the sheared liquid [32]. The applied shear consequently distorts and even destroys local cages formed by neighboring particles, probably leading to anisotropic transports [33–37]. In this nonlinear regime, some widely used conclusions derived from equilibrium, such as the Green-Kubo and Stokes-Einstein (SE) relations, cannot simply be assumed without careful justifications anymore [38,39]. From our literature search, we have not found any previous investigations of isomorphic properties of 3D Yukawa fluids under steady shear, as we will study here.

Dusty plasma, also termed complex plasma, typically refers to partially ionized gas containing micron-sized dust particles [40–52]. In the typical laboratory conditions, these dust particles are charged to thousands or tens of thousands of elementary charges negatively within microseconds in steady state [40,41], interacting with each other through the Yukawa repulsion [42,53]. Due to the high charge on each dust particle, the potential energy between neighboring dust particles is much larger than the kinetic energy, leading to strong coupling between dust particles [54,55], so that dust particles exhibit typical properties of solids and liquids [56–69]. In dusty plasma experiments performed on the space station, dust particles occupy three-dimensional (3D) space, forming 3D dusty plasma [70–72]. During experiments, the motion of individual particles can be directly recorded using video imaging, and then analyzed using particle tracking velocimetry [73,74]. As a result, dusty plasma can be used as an experimental model system [41,45], in which various fundamental procedures can be investigated at the kinetic level. From the previous investigations of dusty plasmas, it is found that 3D dusty plasma liquids, or equivalently 3D Yukawa liquidlike fluids, exhibit isomorph invariance in the structure [75], transport [76], thermodynamic phase diagram [10], and transverse sound speed [76].

In this paper, we investigate isomorphic properties of sheared 3D Yukawa liquidlike fluids using computer simulations. In Sec. II, we provide the isomorph reduced units for various physical quantities. In Sec. III, we describe our

[*]Contact author: fengyan@suda.edu.cn

simulation methods for sheared 3D Yukawa fluids and provide the calculation method of the configurational temperature. In Sec. IV, we report our discovery of the isomorphic scaling properties of shear viscosity and radial distribution function (RDF) of sheared 3D Yukawa liquidlike fluids. We also calculate the diffusion coefficient in this system and find that the Stokes-Einstein relation is violated at higher shear rates. In Sec. V, we provide a summary of our findings.

II. FORMULATIONS IN ISOMORPH THEORY

For R-simple liquids [1–3], the isomorph theory predicts that various structural and dynamical quantities expressed in properly reduced units are approximately invariant along isomorph curves in the phase diagram. According to the isomorph theory [1,3], the units of length, time, and energy for 3D systems are $n^{-1/3}$, $n^{-1/3}\sqrt{m/k_BT}$, and k_BT, respectively. Here, n, m, and T are the number density, the mass of each particle, and the kinetic temperature of the studied system, respectively.

Using this normalization method from the isomorph theory, physical quantities at different states can be compared on the same basis. For the sheared 3D Yukawa fluids studied here, we follow the isomorph theory to normalize the shear viscosity η, shear rate $\dot{\gamma}$, and diffusion coefficient D as

$$\tilde{\eta} = \frac{\eta}{n^{2/3}\sqrt{mk_BT}}, \tag{1}$$

$$\tilde{\dot{\gamma}} = \dot{\gamma} n^{-1/3}\sqrt{\frac{m}{k_BT}}, \tag{2}$$

$$\tilde{D} = Dn^{1/3}\sqrt{\frac{m}{k_BT}}, \tag{3}$$

respectively. To quantify the coupling between shear viscosity and diffusion, we also calculate the dimensionless SE coefficient as

$$\alpha_{\rm SE} = \frac{D\eta n^{-1/3}}{k_BT}. \tag{4}$$

As derived in Ref. [39], for dense 3D liquids close to equilibrium, this SE coefficient is expected to be approximately constant, since viscosity and diffusion are controlled by the closely related local relaxation processes. More specifically, the Zwanzig approximation can be expressed as $\alpha_{\rm SE} \simeq 0.132[1 + c_t^2/(2c_l^2)]$, where c_t and c_l are the transverse and longitudinal high-frequency sound speeds, respectively [77]. For the soft and long-ranged interactions, like the 3D Yukawa repulsion studied here, c_l is typically much larger than c_t, so that the term of $c_t^2/(2c_l^2)$ is negligible, leading to $\alpha_{\rm SE} \simeq 0.132$ for near-equilibrium 3D Yukawa fluids. Note that the physical dependence of $\alpha_{\rm SE}$ on the properties of various liquid systems with different particle interactions has been investigated [78,79].

We also quantify the correlation between the virial and potential energy using the Pearson correlation coefficient [1,2], which is defined as

$$R = \frac{\langle \Delta U \Delta W\rangle}{\sqrt{\langle(\Delta U)^2\rangle\langle(\Delta W)^2\rangle}}. \tag{5}$$

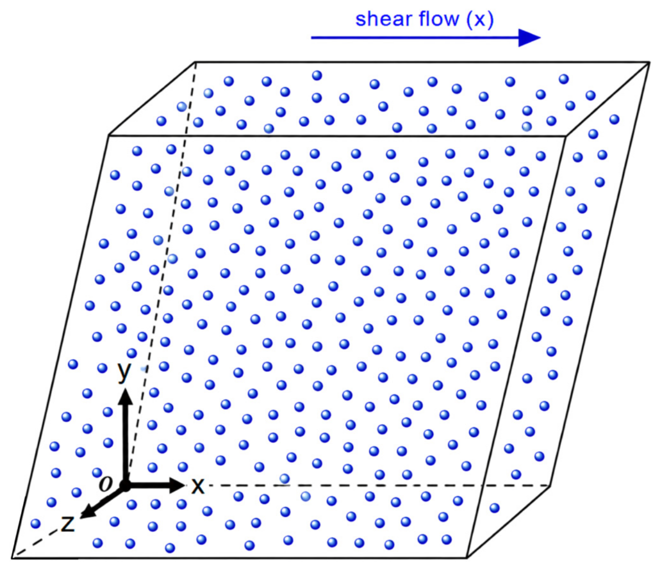

FIG. 1. Schematic illustration of our simulated 3D Yukawa fluid under steady shear. The flow, velocity-gradient, and vorticity directions are chosen along the x, y, and z axes, respectively. The imposed streaming velocity varies linearly with the y coordinate as $u_x(y) = \dot{\gamma} y$, producing a homogeneous shear flow throughout the 3D simulation box.

Here, U is the potential energy, W is the configurational virial, and $\Delta A = A - \langle A\rangle$ denotes the instantaneous fluctuation of quantity A around its steady-state average $\langle A\rangle$. A value of R close to unity indicates the strong correlation between the instantaneous virial and potential-energy fluctuations, which is the typical thermodynamic signature of the R-simple behavior [2].

III. METHODS

A. Nonequilibrium MD simulation using SLLOD

To investigate physical properties of sheared 3D Yukawa fluids, we perform nonequilibrium molecular dynamical (NEMD) simulations using the SLLOD (the reversed spelling of DOLLS [80]) equations of motion [29,30] with the Lees-Edwards periodic boundary conditions [31]. The shear flow direction is chosen along the x axis, so that the velocity-gradient and vorticity directions are along the y and z axes, respectively, as shown in Fig. 1. Following the SLLOD algorithm [30], the imposed streaming velocity is expressed as

$$\mathbf{u}(\mathbf{r}) = \dot{\gamma} y\hat{\mathbf{e}}_x, \tag{6}$$

where $\dot{\gamma}$ is the applied shear rate. As a result, the velocity of each individual particle can be separated into two portions [30] of the streaming and peculiar parts as

$$\mathbf{v}_i = \dot{\gamma} y_i\hat{\mathbf{e}}_x + \frac{\mathbf{p}_i}{m}, \tag{7}$$

where $\mathbf{p}_i$ is the peculiar momentum of particle i. The SLLOD equations of motion for each particle are [30]

$$\dot{\mathbf{r}}_i = \frac{\mathbf{p}_i}{m} + \dot{\gamma} y_i\hat{\mathbf{e}}_x \tag{8}$$

and

$$\dot{\mathbf{p}}_i = \mathbf{F}_i - \dot{\gamma} p_{iy}\hat{\mathbf{e}}_x - \alpha \mathbf{p}_i. \tag{9}$$

Here, $\mathbf{F}_i$ is the total conservative force acting on the particle i, which is just $-\nabla \sum_{j\neq i}^{N} \phi_{ij}$, i.e., the sum of the interparticle Yukawa repulsive forces for our studied 3D Yukawa fluids. On the right-hand side of Eq. (9), α is the Nosé-Hoover thermostat variable applied only to the peculiar momenta, so that the heat generated by viscous heating is removed without directly damping the imposed streaming motion [30].

The SLLOD method plays an important role in our current investigation of sheared 3D Yukawa fluids. For the boundary-driven Couette flow systems, the shear flow is usually generated by moving walls or localized external forces [30], leading to the location-dependent physical quantities, such as the shear rate, temperature, and density. As a result, only one portion of the studied system, where the resulting flow is nearly linear, can be easily used for the data analysis [30]. However, the SLLOD method introduces the uniform velocity gradient directly into the equations of motion for all individual particles. Combined with the Lees-Edwards boundary condition, the SLLOD method generates a homogeneous bulk shear flow, so that various nonideal features in flow systems, such as the wall-induced layering, slip, boundary heating, and density inhomogeneity, are all eliminated.

Based on the SLLOD method described above, we perform NEMD simulations of 3D sheared Yukawa fluids using LAMMPS [81]. Each simulation run contains $N = 8192$ particles in a 3D box, as shown in Fig. 1. Particles interact with each other through the Yukawa repulsion $\phi(r) = Q^2 \exp(-r/\lambda_D)/(4\pi\epsilon_0 r)$ [40,53], reasonably truncated at $15a$ [82], where $a = (3/4\pi n)^{1/3}$ is the Wigner-Seitz radius [53], while Q and λ_D are the dust charge and the Debye length, respectively. The studied 3D Yukawa fluids are characterized by two dimensionless parameters, i.e., the screening parameter $\kappa = a/\lambda_D$ and the coupling parameter $\Gamma = Q^2/(4\pi\epsilon_0 a k_B T)$ [53].

The conditions of our studied 3D sheared Yukawa fluids are listed below. We specify $\kappa = 1$, 2, and 3, which span the typical screening-parameter range in dusty plasma experiments [40,41]. For each value of κ, the coupling parameter is set to $\Gamma/\Gamma_{\rm m} = 0.5$, corresponding to the typical liquidlike state [53] at the same reduced distance from the melting point of $\Gamma_{\rm m}$ [10,18]. In fact, to confirm our reported conclusions here are general as Γ/Γ_m varies, besides $\Gamma/\Gamma_m = 0.5$, we also perform quite a few test runs for different values of Γ/Γ_m in the liquidlike regime [69] of 3D Yukawa fluids, while these detailed results are not presented. The reduced shear rate $\dot{\gamma}/(\bar{v}_p/a)$ is varied from 0.09 to 0.9, where $\bar{v}_p = \sqrt{2k_{\rm B}T/m}$. Note that here we follow the tradition [34,35] to normalize the shear rate using $\dot{\gamma}/(\bar{v}_p/a)$, which is equivalent to Eq. (2) with a constant ratio as $\tilde{\dot{\gamma}} = \sqrt{2}(4\pi/3)^{1/3}\dot{\gamma}/(\bar{v}_p/a)$.

Here are details of our simulations. The time step for the equation of motion is chosen as the well-justified value of $0.005\omega_{pd}^{-1}$ for the liquidlike conditions of 3D Yukawa fluids [82], where $\omega_{pd} = (3Q^2/4\pi\epsilon_0 m a^3)^{1/2}$ is the 3D dusty plasma frequency [53,82]. For each simulation run, after the values of κ and Γ are specified, we first integrate the equation of motion for each particle for at least 10^6 steps to reach equilibrium. Next, after applying shear to the simulated 3D system, we integrate the next 10^6 steps using the Nosé-Hoover thermostat to reach the steady sheared state. We then integrate the last 10^6 steps to collect particle positions, velocities, potential energy, and virial for the data analysis reported here. Other simulation details are similar to those in Ref. [76].

Using the simulation data, we calculate the shear viscosity from its definition [22,83,84] of the ratio of the average off-diagonal stress to the imposed shear rate [30],

$$\eta = -\frac{\langle P_{xy}\rangle}{\dot{\gamma}}. \tag{10}$$

Here, $P_{xy} = [\sum_i (p_{ix}p_{iy}/m) + \sum_{i<j} r_{ij,x}F_{ij,y}]/V$, where the two terms on the right-hand side are the kinetic and virial contributions, respectively. Note that only the peculiar momenta are used in the kinetic part, while the streaming motion has been prescribed by Eq. (6). The use of the stress-to-shear-rate ratio in Eq. (10) agrees with the previous investigation of shear-induced melting of two-dimensional (2D) dusty plasmas, where the drift motion is also removed to determine the shear viscosity using the generalized Green-Kubo relation [37].

B. Configurational temperature

For systems far from thermodynamic equilibrium, temperatures defined from different microscopic degrees of freedom are not necessarily identical [85,86]. For a system under a steady shear, the kinetic temperature obtained from the peculiar velocity may differ from the temperature associated with the particle configuration [87]. Furthermore, due to applied shear flow in one direction, the system has three different Cartesian directions, which are the flow, velocity-gradient, and vorticity [30], so that the configurational response may become anisotropic [87]. To characterize this response, we calculate the configurational temperature separately along the three Cartesian directions.

The configurational temperature provides a measure of temperature using only particle positions and conservative forces [85,86]. The calculation method of the configurational temperature follows the general statistical-mechanical formulation of temperature introduced by Rugh [85]. For one studied system with the total interaction potential energy of $U(\mathbf{R}) = \sum_{i<j}\phi(r_{ij})$, its configurational probability ρ in equilibrium can be expressed as $\rho(\mathbf{R}) = \exp[-U(\mathbf{R})/(k_B T)]/Z$, where Z is the partition function [22]. Following the derivation provided in detail in Refs. [85,86], one may obtain the expression of $\langle \partial^2 U/\partial q^2\rangle = (k_B T)^{-1}\langle(\partial U/\partial q)^2\rangle$ for any configurational coordinate q. This relation shows that temperature can be determined from the gradient and curvature of the potential-energy landscape, without using the velocity data [86].

Following the relation described above separately along various directions, we calculate different components of the configurational temperature [87] for our studied 3D Yukawa fluids using

$$k_B T_{{\rm conf},\beta} = \frac{\left\langle \sum_{i=1}^{N} F_{i\beta}^2\right\rangle}{\left\langle -\sum_{i=1}^{N} \frac{\partial F_{i\beta}}{\partial r_{i\beta}}\right\rangle}, \quad \beta = x, y, z. \tag{11}$$

Here, $F_{i\beta} = -\partial U/\partial r_{i\beta}$ is the β component of the total conservative Yukawa force on the particle i, while $\langle \cdots \rangle$ denotes the ensemble average in the steady state. The denominator of Eq. (11) measures the corresponding curvature summation of the potential-energy landscape [85], while the numerator seems to be the summation of the square of the component of the Yukawa force along the studied direction. From Ref. [85], the configurational temperature can be regarded as the configurational energy scale sampled by the particles.

In the SLLOD simulations used in our current study, the applied Nosé-Hoover thermostat regulates the kinetic temperature calculated from the peculiar velocities only. As a result, Eq. (11) depends only on the instantaneous particle configuration and conservative Yukawa forces [87]. From Refs. [85,86], in thermal equilibrium, both the configurational and kinetic temperatures are the same as the thermodynamic temperature, i.e., $T_{\mathrm{conf},x} = T_{\mathrm{conf},y} = T_{\mathrm{conf},z} = T_{\mathrm{kin}}$. For the SLLOD simulation results, the departure of $T_{\mathrm{conf},\beta}/T_{\mathrm{kin}}$ from unity therefore indicates a nonequilibrium separation between the configurational and kinetic degrees of freedom. Furthermore, the difference between the three directional components of the configurational temperature further reveals an anisotropic deformation of the local cages formed by neighboring particles [87]. In fact, the directional configurational temperatures can be used as structural diagnostics of sheared substances [87], rather than as three independent thermodynamic temperatures.

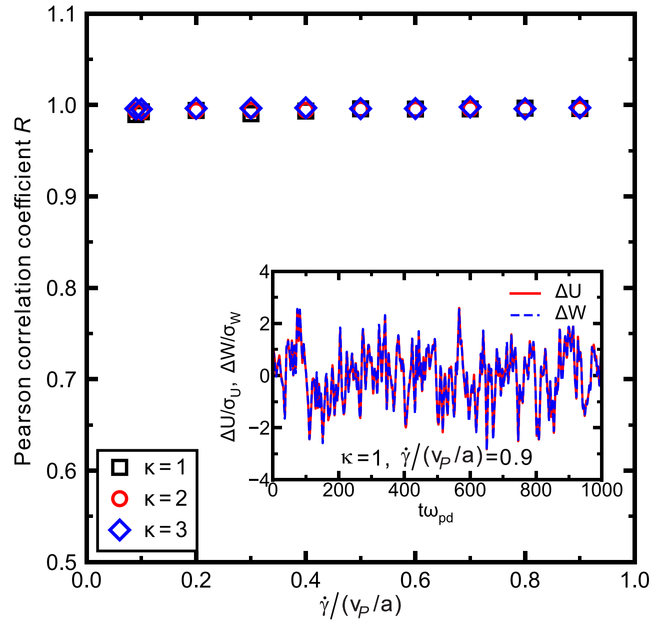

FIG. 2. Calculated Pearson correlation coefficient R between the instantaneous potential-energy fluctuation ΔU and virial fluctuation ΔW for sheared 3D Yukawa fluids of $\kappa = 1$, 2, and 3, as a function of the reduced shear rate $\dot{\gamma}/(\bar{v}_p/a)$. The inset shows the normalized fluctuations of $\Delta U/\sigma_U$ and $\Delta W/\sigma_W$ for the conditions of $\kappa = 1$ and $\dot{\gamma}/(\bar{v}_p/a) = 0.9$, where σ_U and σ_W are the standard deviations of U and W, respectively. Clearly, the R value is always very close to unity for all studied conditions, indicating the strong correlation between ΔU and ΔW for 3D Yukawa fluids under steady shear.

IV. RESULTS AND DISCUSSION

A. Thermodynamic quantities

To test whether the isomorph theory is still applicable for our studied systems, we first calculate the Pearson correlation coefficient R of sheared 3D Yukawa liquidlike fluids using Eq. (5), as presented in Fig. 2. Interestingly, for all of the studied conditions here, our calculated R values are all very close to unity. From the inset of Fig. 2, for the conditions of $\dot{\gamma}/(\bar{v}_p/a) = 0.9$ and $\kappa = 1$, the time series of fluctuations of the normalized potential energy ΔU and virial ΔW almost completely overlap together. Clearly, the synchronized fluctuations ΔU and ΔW reasonably lead to the nearly unity Pearson correlation coefficient R in Fig. 2, suggesting that the isomorph theory may still be applicable for sheared 3D Yukawa fluids.

From our understanding, the strong correlation between U and W in sheared 3D Yukawa liquidlike fluids in Fig. 2 probably originates from the same near-neighboring configurations governing both quantities. For equilibrium R-simple liquids, the hidden scale invariance implies that the same changes in interparticle separations generate proportional fluctuations of the potential energy and virial [3,13,14]. In the present nonequilibrium systems, shear-induced rearrangements of the cages formed by neighboring particles modify the local interparticle separations, so that the potential energy and virial are also changed simultaneously. This interpretation agrees with the isomorph invariance of Couette shear flows generated by the SLLOD equations under the fixed reduced shear rate, as demonstrated in Ref. [25]. Since 3D Yukawa liquidlike fluids are typical R-simple systems [75,76], the applied shear does not destroy the strong U-W correlation. As a result, the sheared 3D Yukawa fluids are also R-simple liquids, i.e., the isomorph theory is still applicable for the systems studied here.

To study the anisotropic configurational response of our studied sheared 3D Yukawa fluids, we calculate $T_{\mathrm{conf},\beta}$ using Eq. (11), with the results presented in Fig. 3. From Fig. 3, as the shear rate increases, besides the general decline trend of the configurational temperature, we also observe that more significant separation of different components of the configurational temperature for sheared 3D Yukawa liquidlike fluids. At the lowest shear rate of $\dot{\gamma}/(\bar{v}_p/a) = 0.09$, for the three components of the configurational temperature, the ratio of $T_{\mathrm{conf}}/T_{\mathrm{kin}}$ is always close to unity, no matter how κ varies. In Figs. 3(a)–3(c), as the shear rate $\dot{\gamma}/(\bar{v}_p/a)$ increases, the three ratios of $T_{\mathrm{conf},xyz}/T_{\mathrm{kin}}$ decrease gradually and also separate more significantly. For each κ value, the x component of the configurational temperature $T_{\mathrm{conf},x}$ is always the highest, while its z component $T_{\mathrm{conf},z}$ is generally the lowest. This ordering of the three components of the configurational temperature demonstrates that the shear-induced distortion is not a uniform reduction of the configurational temperature, but a genuinely anisotropic force-field response.

Besides the general trend of the configurational temperature described above, we also observe that the configurational temperature at higher shear rates exhibits the dependence on the screening parameter κ. For $\kappa = 1$ in Fig. 3(a), as the shear rate increases, $T_{\mathrm{conf},x}/T_{\mathrm{kin}}$ decays substantially and approaches

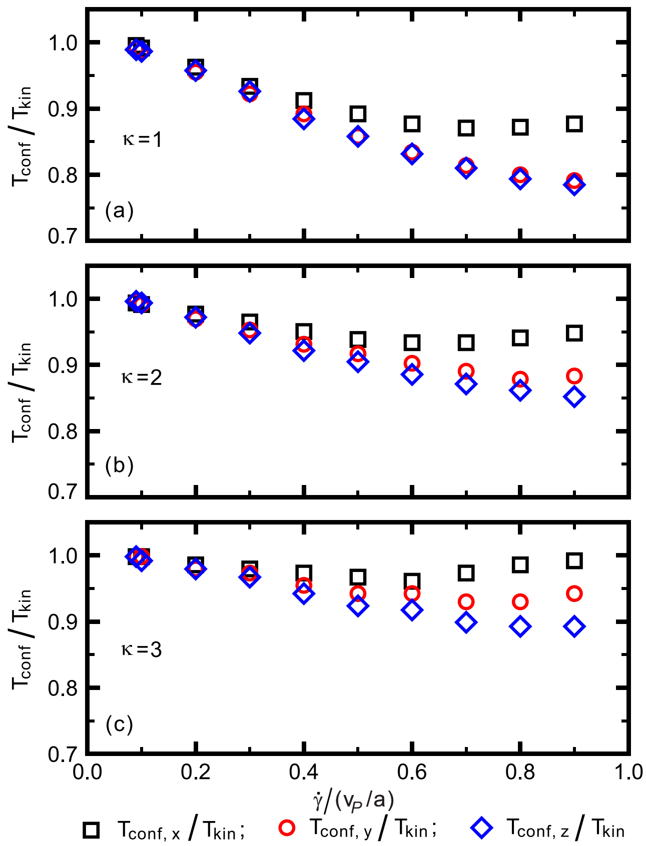

FIG. 3. Calculated ratio of the directional configurational temperature to the kinetic temperature $T_{\mathrm{conf},\beta}/T_{\mathrm{kin}}$ under various shears for 3D Yukawa fluids of $\kappa = 1$ [panel (a)], $\kappa = 2$ [panel (b)], and $\kappa = 3$ [panel (c)] from our simulation data. Here, the configurational temperature $T_{\mathrm{conf},\beta}$ is calculated using Eq. (11) from the local conservative force field, while T_{kin} is determined from the peculiar thermal motion. Clearly, as the shear rate $\dot{\gamma}$ increases, the ratio of $T_{\mathrm{conf},\beta}/T_{\mathrm{kin}}$ decreases slightly from unity to ≈0.8 at most, while the anisotropy of $T_{\mathrm{conf},\beta}$ becomes more significant gradually.

0.88 gradually, while $T_{\mathrm{conf},y}/T_{\mathrm{kin}}$ and $T_{\mathrm{conf},z}/T_{\mathrm{kin}}$ decrease much more significantly to ≈0.78. For $\kappa = 2$ in Fig. 3(b), when the shear rate increases, $T_{\mathrm{conf},x}/T_{\mathrm{kin}}$, $T_{\mathrm{conf},y}/T_{\mathrm{kin}}$, and $T_{\mathrm{conf},z}/T_{\mathrm{kin}}$ decay and then approach approximately 0.94, 0.88, and 0.85, respectively. For $\kappa = 3$ in Fig. 3(c), as the shear rate gradually increases, $T_{\mathrm{conf},x}/T_{\mathrm{kin}}$ first decreases and then surprisingly increases back to nearly unity, while $T_{\mathrm{conf},y}/T_{\mathrm{kin}}$ and $T_{\mathrm{conf},z}/T_{\mathrm{kin}}$ only decay to about 0.95 and 0.9, respectively. Thus, for our studied configurational temperature of sheared 3D Yukawa fluids, the magnitude of the overall departure from the kinetic temperature decreases with the screening parameter κ.

The variation trends of different components of the configurational temperature for sheared 3D Yukawa fluids presented in Fig. 3 can be explained from the shear-deformed cages formed by neighboring particles described next. For our studied sheared 3D systems illustrated in Fig. 1, the shear flow $u_x = \dot{\gamma} y$ along the x direction directly deforms the local particle cages within the x–y plane. From the principal stress theorem [30,88–91], due to the applied shear along the x direction, our studied 3D Yukawa fluids are stretched in the direction of 45° with respect to the flow direction, and also compressed along the other perpendicular direction, which has been experimentally verified in a 2D complex plasma [92]. The stretching and compressing effects in two perpendicular directions definitely lead to the deformation of cages formed by neighboring particles, or equivalently the anisotropic rearrangement of neighboring particles, thereby modifying the numerator and denominator of the right-hand side of Eq. (11), or the x and y components of the configurational temperature. Although the applied shear does not lead to the direct affine stretching or compression in the z direction [30], the particle motions in three directions are definitely coupled together due to the 3D interparticle force network, so that the cage rearrangements within the shear plane can also modify the configurational response along the z direction. The overall decline trend of $T_{\mathrm{conf},\beta}/T_{\mathrm{kin}}$ with the shear rate indicates that the force fluctuations and potential-energy curvatures no longer retain their equilibrium balance, while the separation of these three components reflects the direction-dependent reorganization of the local force network. Furthermore, as κ increases, the effective distance of the Yukawa repulsion becomes shorter, so that the configurational response becomes more strongly localized around near neighbors. As a result, the local force-curvature balance is less sensitive to the imposed shear, reasonably resulting in the values of $T_{\mathrm{conf},\beta}/T_{\mathrm{kin}}$ closer to unity for larger κ values, as shown in Fig. 3.

B. Isomorphic property of structure under shear

We calculate the RDF $g(r)$ of sheared 3D Yukawa fluids under various conditions, as presented in Fig. 4. The RDFs in these three panels of Fig. 4 correspond to the three representative reduced shear rates of $\dot{\gamma}/(\bar{v}_p/a) = 0.1$, 0.5, and 0.8, while the value of $\Gamma/\Gamma_{\mathrm{m}}$ is kept unchanged as 0.5 for the easy comparison. Note that, for the typical shear-induced melting dusty plasma experiment [93] of $\dot{\gamma} = 0.0789\,\omega_{pd}$, the value of $\dot{\gamma}/(\bar{v}_p/a) \approx 0.1$, so that the largest reduced shear rate $\dot{\gamma}/(\bar{v}_p/a) = 0.8$ studied here corresponds to about one order of magnitude more powerful shear flow than that for the typical dusty plasma experiments [93].

From Fig. 4, for each studied shear rate, our obtained $g(r)$ results of $\kappa = 1$, 2, and 3 almost completely collapse together. For the lowest shear rate of $\dot{\gamma}/(\bar{v}_p/a) = 0.1$, from Fig. 4(a), the first peak, the first minimum, and the subsequent oscillations of the three $g(r)$ curves are almost completely identical. The same agreement is also clearly observed for the three $g(r)$ results at the intermediate shear rate of $\dot{\gamma}/(\bar{v}_p/a) = 0.5$ in Fig. 4(b). For the $g(r)$ results of $\dot{\gamma}/(\bar{v}_p/a) = 0.8$ in Fig. 4(c), their agreement is also undoubted, although the height of the first peak varies very slightly ≈0.012 for different κ values. Our observed collapse of the $g(r)$ results under various conditions in Fig. 4 definitely indicates that the angle-averaged local structure is invariant for various κ values at the same reduced shear rate, clearly demonstrating the isomorphic property of the structure of our studied sheared 3D Yukawa fluids.

Besides the collapse of the $g(r)$ results for different κ values described above, we also observe the slight difference of $g(r)$ as the shear rate increases in Fig. 4. From Figs. 4(a)–4(c), as the reduced shear rate $\dot{\gamma}/(\bar{v}_p/a)$ increases from 0.1 to 0.8, the height of the first peak decreases slightly from

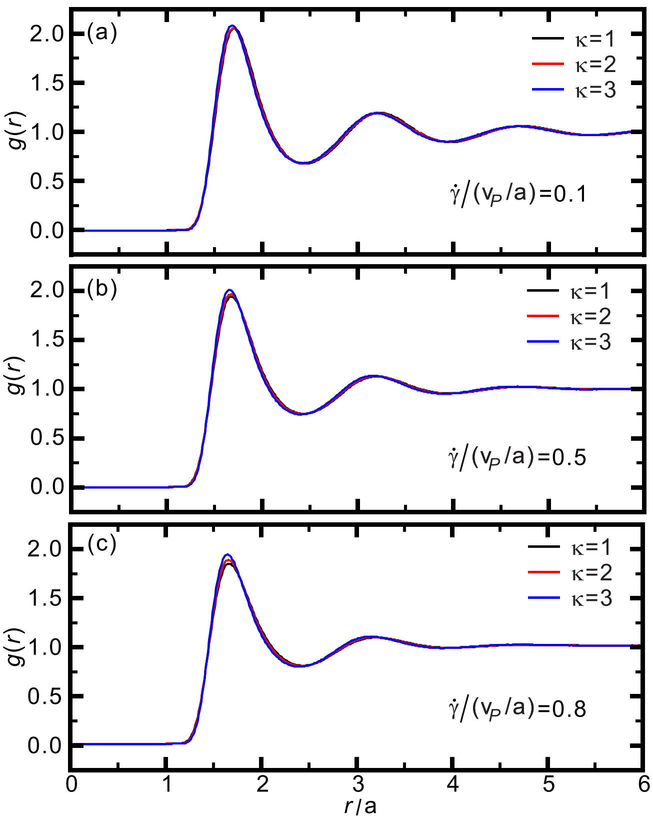

FIG. 4. Calculated radial distribution functions $g(r)$ of 3D Yukawa fluids for varying κ values at the same reduced coupling strength $\Gamma/\Gamma_{\rm m} = 0.5$, under three representative reduced shear rates of $\dot{\gamma}/(\bar{v}_p/a) = 0.1$ [panel (a)], 0.5 [panel (b)], and 0.8 [panel (c)], respectively. Clearly, as the shear rate varies, the obtained $g(r)$ results of 3D Yukawa fluids for different κ values almost collapse to one universal curve in reduced units, indicating that the radial local structure is approximately invariant. Note that, when $\dot{\gamma}$ increases, the height of the first peak of $g(r)$ varies very slightly $\approx$0.012 for different κ values, as shown in panel (c), probably due to the significant configurational distortion in Fig. 3 modifying the averaged isotropic structure measure of $g(r)$.

$\approx$2.09 to $\approx$1.87. Furthermore, the subsequent oscillations of $g(r)$ become moderately weaker for higher shear rates. The decrease of the first peak height and the weaker subsequent oscillations both indicate that the angle-averaged translational order of our studied sheared 3D Yukawa fluids is reduced when the shear rate is higher. Note that the collapse of the $g(r)$ results and their variation trends for all other studied shear rates not reported here are quite similar to those in Fig. 4. Note that, besides the global angle-averaged $g(r)$ results reported above, to better characterize the shear-distorted structure, we also perform quite a few tests using the structural diagnostic of the angle-resolved pair correlation function [94] in the shear plane, which also indicate the isomorphic property of the distorted structure of our studied sheared 3D Yukawa fluids.

From our understanding, the collapse of the $g(r)$ results in Fig. 4 indicates nearly the same particle arrangement in the reduced units for the studied 3D Yukawa fluids while the relative coupling parameter $\Gamma/\Gamma_{\rm m}$ and the reduced shear rate are unchanged. Although the directional configurational temperatures in Fig. 3 exhibit the pronounced anisotropic response, the calculated RDF averages the pair distribution over all directions; i.e., this directional distortion cannot be easily reflected by the $g(r)$ results. As a result, the applied shear redistributes the configurational correlations among different directions while leaving their radial average nearly unchanged for different κ values. In fact, the results in Figs. 3 and 4 therefore describe two complementary aspects of the same local structure due to the applied shear.

C. Isomorphic property of viscosity under shear

Based on our SLLOD simulation data at different shear rates, we calculate the shear viscosity η of 3D Yukawa fluids with the relative coupling parameter of $\Gamma/\Gamma_m = 0.5$ using the constitutive relation of Eq. (10), as plotted in Fig. 5(a). From Fig. 5(a), the obtained viscosity data exhibit a pronounced dependence on the screening parameter κ. For the same shear rate, as κ increases from 1 to 3, the viscosity of the sheared 3D Yukawa fluids decreases substantially. For example, when $\dot{\gamma}/(\bar{v}_p/a) = 0.5$, our obtained values of $\eta/(nma^2\omega_{\rm pd})$ are approximately 0.120, 0.086, and 0.054 for $\kappa = 1$, 2, and 3, respectively. We attribute this decreasing trend of shear viscosity with the screening parameter to the more screened interparticle interaction of our studied sheared Yukawa fluids for larger κ values, or particle interaction is more localized, so that the momentum transport is less efficient, reasonably leading to a lower value of shear viscosity.

From Fig. 5(a), for each value of κ, the viscosity always decreases monotonically with the shear rate, just corresponding to the typical non-Newtonian shear-thinning behavior [33–35]. For example, when $\kappa = 2$, the calculated $\eta/(nma^2\omega_{\rm pd})$ decreases monotonically from $\approx$0.108 at $\dot{\gamma}/(\bar{v}_p/a) = 0.1$ to $\approx$0.071 at $\dot{\gamma}/(\bar{v}_p/a) = 0.9$. The decreasing trend of the shear viscosity with the shear rate is general for other screening parameters, as those for $\kappa = 1$ and 3 presented in Fig. 5(a). We attribute the decreasing of shear viscosity with the shear rate to the fact that cages formed by neighboring particles are significantly deformed and rearranged at higher shear rates, reducing the ability to sustain shear and transfer momentum, corresponding to lower values of shear viscosity.

As the major result of this paper, we discover that, when the viscosity is normalized using the isomorph reduced units as in Eq. (1), all viscosity data points almost collapse onto a universal curve, completely independent of the screening parameter κ, as presented in Fig. 5(b). This scaling collapse demonstrates that the shear viscosity of 3D Yukawa fluids remains approximately isomorph invariant even though the studied fluids are driven away from equilibrium by steady shears. It also indicates that the pronounced κ dependence of viscosity observed in Fig. 5(a) mainly originates from the conventional constant units used in dusty plasmas, rather than from an intrinsic difference in the reduced rheological response. Therefore, the hidden scale invariance governing the equilibrium transport properties of 3D Yukawa liquidlike fluids [95] continues to control their nonlinear shear-thinning behavior under nonequilibrium conditions.

We attribute the observed collapse of the viscosity data in Fig. 5(b) to the dominant role of neighboring particles in the momentum transport of shear viscosity. From the previous

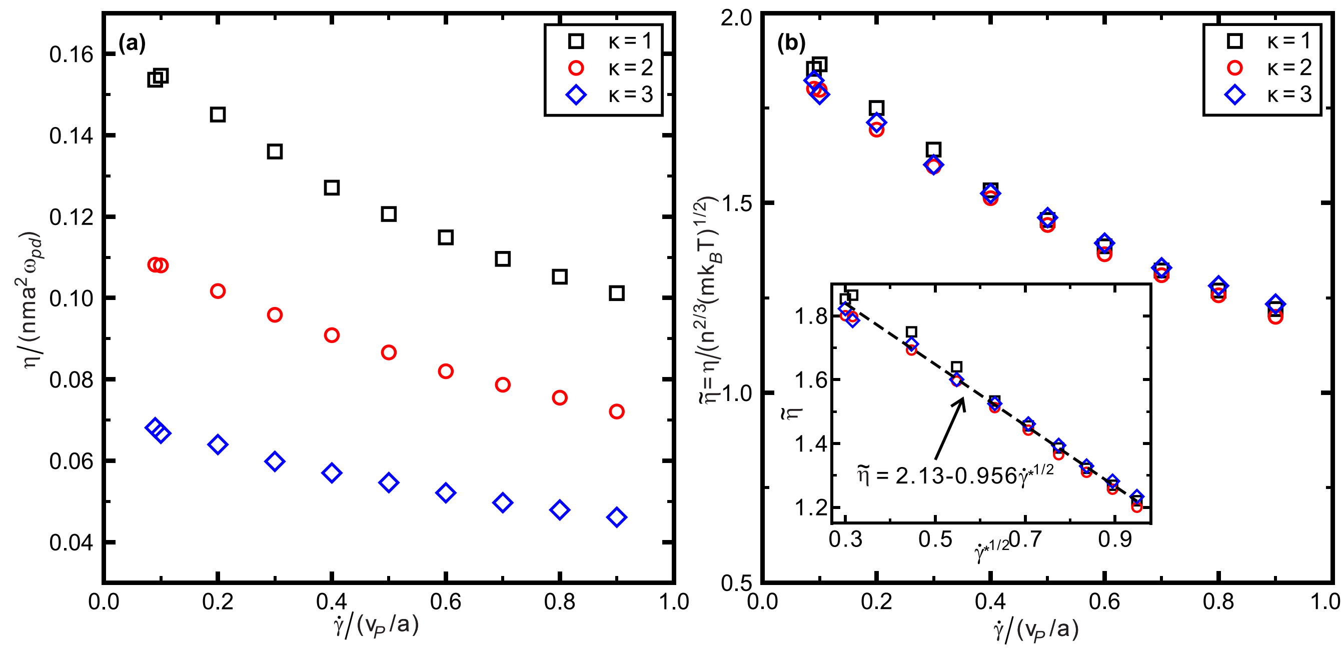

FIG. 5. Obtained shear viscosity η of 3D Yukawa fluids with the fixed relative coupling parameter $\Gamma/\Gamma_m = 0.5$ under steady shears for $\kappa = 1$, 2, and 3 from our simulations, plotted in the reduced units of $nma^2\omega_{pd}$ [panel (a)] and the isomorph reduced units of $n^{2/3}(mk_BT)^{1/2}$ [panel (b)], respectively. From panel (a), clearly, as $\dot{\gamma}$ increases, the 3D Yukawa fluids for each κ value always exhibit the typical non-Newtonian shear-thinning behavior. While we normalize the viscosity using the isomorph reduced units as in panel (b), remarkably, all data points of $\eta/n^{2/3}(mk_BT)^{1/2}$ of 3D Yukawa fluids for various κ values nearly collapse into one for each shear rate value. This collapse of data points in panel (b) clearly indicates that the viscosity of sheared 3D Yukawa liquidlike fluids remains approximately isomorph invariant. In the inset in panel (b), the calculated reduced viscosity results of $\widetilde{\eta}$ are replotted as the function of $\dot{\gamma}^{*1/2} = (\dot{\gamma}/(\bar{v}_p/a))^{1/2}$ using the same data. Clearly, the exhibited linear decrease of the reduced viscosity $\widetilde{\eta}$ with $\dot{\gamma}^{*1/2}$ leads to the linear fitting result, obtained by fitting all data for $\kappa = 1$, 2, and 3 with $\dot{\gamma}^{*1/2} \geqslant 0.6$, as the dashed line shown there.

investigation of 2D simple liquidlike fluids, shear viscosity is determined completely by rearrangement of neighboring particles [95,96]. We speculate that the viscosity mechanism of our studied 3D Yukawa liquidlike fluids is probably similar to that for 2D liquidlike fluids, i.e., the viscosity of 3D Yukawa liquidlike fluid is probably also mainly determined by neighboring particles. With the same relative coupling parameter and the same reduced shear rate, even though the κ value varies, the studied 3D Yukawa liquidlike fluids exhibit the same local structure in the isomorph reduced units, as the $g(r)$ results shown in Fig. 4. When these same structures in Fig. 4 are subjected to the same reduced shear rate, our studied 3D Yukawa fluids therefore undergo the similar deformation of cages formed by neighboring particles and then the rearrangement during the same reduced time interval, reasonably leading to the same reduced viscosity expressed in the isomorphic units, no matter how κ varies, as shown in Fig. 5(b).

To further investigate the shear dependence of viscosity for our studied 3D Yukawa liquidlike fluids, in the inset of Fig. 5(b), we present the same isomorph-reduced viscosity data $\widetilde{\eta} = \eta/[n^{2/3}(mk_BT)^{1/2}]$ as a function of $\dot{\gamma}^{*1/2} = (\dot{\gamma}/(\bar{v}_p/a))^{1/2}$ instead. Clearly, over the entire studied range of shear rate, $\widetilde{\eta}$ decreases approximately linearly with $\dot{\gamma}^{*1/2}$, as indicated by the dashed line there. This dashed line is obtained from the simultaneous linear fit using all 18 data points for $\kappa = 1$, 2, and 3 with $\dot{\gamma}^{*1/2} \geqslant 0.6$, leading to $\widetilde{\eta} = 2.13 - 0.956\dot{\gamma}^{*1/2}$. This fitting expression is also able to accurately describe the remaining viscosity data of $\dot{\gamma}^{*} \geqslant 0.09$; however, we do not expect this fitting can be extrapolated further to lower shear rates, where the viscosity is nearly unchanged from [35]. Thus, the viscosity of our studied 3D Yukawa liquidlike fluids without shear can be estimated as the reduced viscosity of $\widetilde{\eta} \approx 1.8$ when $\dot{\gamma}^{*} = 0.09$, very close to the equilibrium estimation of $\widetilde{\eta} \simeq 0.126\exp[3.64\sqrt{\Gamma/\Gamma_m}] \simeq 1.7$ for $\Gamma/\Gamma_m = 0.5$ obtained from the practical formula proposed in Ref. [97]. Note that our normalized shear rate $\dot{\gamma}^{*} = \dot{\gamma}/(\bar{v}_p/a)$ is equivalent to the isomorph-reduced shear rate of Eq. (2) with a constant factor, i.e., $\widetilde{\dot{\gamma}} = \sqrt{2}(4\pi/3)^{1/3}\dot{\gamma}^{*} \simeq 2.28\dot{\gamma}^{*}$.

Our use of $\dot{\gamma}^{*1/2}$ for the horizontal axis of the inset of Fig. 5(b) is motivated by the previous theoretical studies connecting nonlinear viscosity with long-time hydrodynamic correlations [98–100]. In equilibrium 3D systems, the long-wavelength hydrodynamic fluctuations decay slowly, allowing the fluid to retain a memory of the shear stress and producing a $t^{-3/2}$ long-time tail [99]. Under steady shear, the flow continuously stretches and tilts these large-scale fluctuation patterns, so that they lose memory of their initial states once the accumulated strain becomes of order unity as $|\dot{\gamma}|t \sim 1$ [101]. The corresponding shear-advection time $t_\gamma \sim |\dot{\gamma}|^{-1}$ therefore limits the duration over which these slow fluctuations contribute to the viscosity [101]. The mode-coupling [98] and ring-kinetic theories [99,100] show that this suppression of the 3D long-time tail gives rise to a nonanalytic viscosity correction $\propto |\dot{\gamma}|^{1/2}$ [98,99]. Although this result is not a rigorous constitutive law for our present studied 3D Yukawa liquidlike

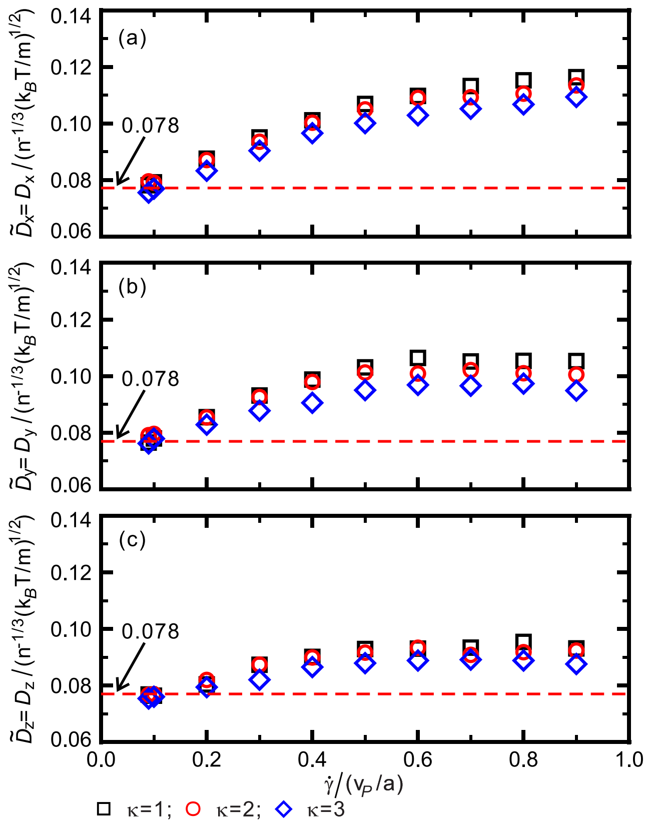

FIG. 6. Calculated diffusion coefficients D, normalized by the isomorph units of $n^{-1/3}(k_BT/m)^{1/2}$, for 3D Yukawa fluids under steady shear in the flow direction [panel (a)], the velocity-gradient direction [panel (b)], and the vorticity direction [panel (c)], for $\kappa = 1$, 2, and 3, respectively. Clearly, for the lower shear rates, the normalized diffusion coefficients in all three directions converge to ≈0.078 for different κ values, demonstrating that the diffusion coefficient obeys the isomorphic scaling in the near-equilibrium state. However, as the shear rate increases, the normalized diffusion coefficients explicitly exhibit both the directional and κ dependence, suggesting that strong shear leads to the anisotropy of the studied system, and the diffusion coefficient is not an isomorphic invariant anymore.

fluids, it provides an empirical fitting $\widetilde{\eta} = \widetilde{\eta}_0 - A\dot{\gamma}^{*1/2}$ to the observed shear-thinning behavior, as also observed in our studied sheared 3D Yukawa liquidlike fluids from the inset of Fig. 5(b).

D. Diffusion under shear and breakdown of Stokes-Einstein relation

We also calculate the diffusion coefficient of our studied sheared 3D Yukawa fluids using the SLLOD simulation data, as presented in Fig. 6. In fact, the diffusion property characterized by the mean-squared displacement (MSD) in equilibrium 3D Yukawa fluids has been demonstrated to be isomorph invariant in reduced units [76]. However, whether the applied shear is able to destroy the invariance of the diffusion property in 3D Yukawa fluids is still an open problem, as we study here. To characterize the diffusion property, based on the SLLOD simulation data, we calculate the directional diffusion coefficients from the long-time MSD using

$$D_\beta = \lim_{t\to\infty} \frac{\langle[\Delta r_\beta(t)]^2\rangle}{2t}, \quad \beta = x, y, z. \tag{12}$$

Here, $\langle\rangle$ denotes the ensemble average. In the velocity-gradient and vorticity directions, Δr_β is just the displacement of particles in the y and z directions. However, in the flow direction, to calculate Δr_x, the flow motion generated by the imposed shear should be removed, i.e., $\Delta r_x(t) = x(t) - x(0) - \dot{\gamma}\int_0^t y(t')\,dt'$ [30]. We also normalize the calculated diffusion coefficients using the isomorphic units as in Eq. (3).

From Fig. 6, our obtained diffusion coefficients of sheared 3D Yukawa fluids for all three directions in the reduced units generally increase with the shear rate. At the lowest shear rate, the nine data points of the dimensionless diffusion coefficient are all very close to 0.078, which is just the reduced diffusion coefficient of equilibrium 3D Yukawa fluid at the same relative coupling parameter $\Gamma/\Gamma_m = 0.5$ from the previous investigation of Ref. [76]. As the shear rate increases, $\widetilde{D}_x$, $\widetilde{D}_y$, and $\widetilde{D}_z$ all increase gradually from ≈0.078 to higher values. It seems that the applied shear significantly enhances the diffusion of our studied 3D Yukawa fluids, as discussed in detail later.

Besides the general increase trend in Fig. 6, we also observe the directional anisotropy and the screening-parameter dependence of the diffusion coefficient for our studied systems. In the flow direction, from Fig. 6(a), $\widetilde{D}_x$ exhibits the most significant enhancement with the shear rate, reaching ≈0.11 at the highest shear rate of $\dot{\gamma}/(\bar{v}_p/a) = 0.9$. However, in the vorticity direction, $\widetilde{D}_z$ exhibits the least increase with the shear rate, reaching only ≈0.098 when $\dot{\gamma}/(\bar{v}_p/a) = 0.9$, as shown in Fig. 6(c). In the velocity-gradient direction, the increase of $\widetilde{D}_y$ is in the intermediate level. Clearly, the resulting order of $\widetilde{D}_x > \widetilde{D}_y > \widetilde{D}_z$ demonstrates that the diffusion of sheared 3D Yukawa fluids exhibits the prominent anisotropic feature. At the same time, the diffusion coefficient for different screening parameters also varies. From Fig. 6, while other conditions are the same, the diffusion coefficient for $\kappa = 1$ is generally larger than that for $\kappa = 2$, while diffusion coefficient for $\kappa = 3$ is the lowest. Probably this screening-parameter dependence of the diffusion coefficient can also be attributed to the more localized effect of the Yukawa interaction for larger κ values, as we discuss for the viscosity results above. Thus, although the diffusion coefficient is a widely accepted invariant from the isomorph theory [3], our results in Fig. 6 clearly indicate that the applied shear substantially destroys the invariance of the diffusion coefficient for 3D Yukawa fluids, which exhibits both the directional and κ dependence.

Our observed variation trend of diffusion coefficient and its anisotropy in Fig. 6 can be explained by the cumulative shear-assisted decaging motion in 3D Yukawa fluids. The imposed shear flow $u_x = \dot{\gamma}y$ directly deforms cages formed by neighboring particles mainly in the x direction and also enhances the particle velocity in the x direction. Even though the flow displacement due to the applied shear is removed in our calculations, the diffusion along the shear direction is still greatly enhanced at higher shear rates, probably suggesting that the flow and peculiar velocities in the x direction are somewhat linked together. The diffusion of particles along the y direction is also substantially modified at higher shear rates, which we attribute to the coupling of particle motion in the x–y plane with the significant shear flow velocity gradient. In principle, the particle motion along the z direction should not be affected by the applied shear, since all parameters are uniform along this direction. However, for 3D Yukawa fluids, the particle motions in all three directions are definitely coupled together, so that it is probably reasonable that the enhanced diffusion in the x and y directions is able to improve the diffusion in the z direction, leading to the least increase of $\widetilde{D}_z$ with the shear rate, as presented in Fig. 6(c).

Since the viscosity and diffusion coefficient of sheared 3D Yukawa fluids are obtained in Figs. 5 and 6 above, we also easily calculate the corresponding SE coefficient, as presented in Fig. 7. In fact, for equilibrium systems, the famous SE relation of $D = k_B T/(c\pi\eta\sigma)$ [22,102,103] provides the balance between the thermal fluctuations driving the Brownian motion and the viscous resistance exerted by the surrounding liquid, where σ is the hydrodynamic diameter [22,102], and c is a constant that depends on the boundary condition at the particle surface [22,102]. As a result, the SE relation establishes a direct connection between the microscopic diffusion and the macroscopic viscosity [22,103]. For dense liquids, it has been demonstrated that the velocity- and stress-correlation functions lead to an analogous relation between diffusion and viscosity, which is $\alpha_{\rm SE} = D\eta n^{-1/3}/k_B T = \text{const}$ [39,104]. For our studied nonequilibrium 3D sheared Yukawa fluids, the product of shear viscosity η and the diffusion coefficient D exhibits different features, as plotted in Fig. 7.

From Fig. 7, as the shear rate increases, the SE-coefficient results exhibit the pronounced anisotropic behavior. In the flow direction, the corresponding SE coefficient $\alpha_{{\rm SE},x}$ does not change substantially with the shear rate, only varying slightly between $\approx$0.156 and $\approx$0.135, as shown in Fig. 7(a). However, from Fig. 7(c), the SE coefficient $\alpha_{{\rm SE},z}$ in the vorticity direction drops almost monotonically from $\approx$0.142 to $\approx$0.108 as the shear rate increases to $\dot{\gamma}/(\bar{v}_p/a) = 0.9$. The variation trend of the SE coefficient $\alpha_{{\rm SE},y}$ in Fig. 7(b) is in the intermediate level, i.e., dropping with the shear rate less than $\alpha_{{\rm SE},z}$. In short, the different variation trends of $\alpha_{{\rm SE},x}$, $\alpha_{{\rm SE},y}$, and $\alpha_{{\rm SE},z}$ clearly indicate that, for our studied sheared 3D Yukawa liquidlike fluids, the SE relation is not obeyed anymore, or the SE relation is violated.

Another interesting point in Fig. 7 is that, at lower shear rates, the SE coefficients in the three directions all converge to $\approx$0.14. In fact, for dense liquids in equilibrium, by substituting the hydrodynamic diameter σ in the SE relation using $2n^{-1/3}$, it has been derived that the SE coefficient should be $\approx$0.132 [77]. For our studied Yukawa fluids with lower shear rates, which should be close to equilibrium, our obtained value of $\alpha_{\rm SE} \approx 0.14$, pretty agreeing with the derived value of $\approx$0.132 [77]. Note that, using the estimated viscosity without shear $\widetilde{\eta}_0 \simeq 1.8$ above, together with $\widetilde{D} \simeq 0.078$ there, we obtain $\alpha_{\rm SE} = \widetilde{D}\widetilde{\eta}_0 \simeq 0.14$, further confirming the consistency among the viscosity, diffusion, and SE-coefficient results under the near-equilibrium condition.

We attribute the breakdown of the SE relation in sheared 3D Yukawa liquidlike fluids to the different variation trends of viscosity and diffusion due to the applied shear. In principle, the SE relation is intended for equilibrium systems [39,103], which is also valid for those near equilibrium [77], so that we do not expect that it is always obeyed for our studied sheared 3D Yukawa fluids far from equilibrium. The macroscopic shear viscosity is governed by the off-diagonal stress tensor P_{xy}, which characterizes the transport of the x-directed momentum across adjacent fluid layers separated along the y direction. Although the shear-thinning effect reduces the viscosity as shown in Fig. 5, the structural rearrangements strongly promote nonaffine particle migration along the flow direction, leading to a substantial enhancement of diffusion coefficient in the flow direction, as shown in Fig. 6. This drastic increase in $\widetilde{D}_x$ in Fig. 6(a) effectively compensates for the drop in $\widetilde{\eta}$ in Fig. 5, leading to the nearly unchanged SE coefficient $\alpha_{{\rm SE},x}$, as shown in Fig. 7(a). In contrast, the particle

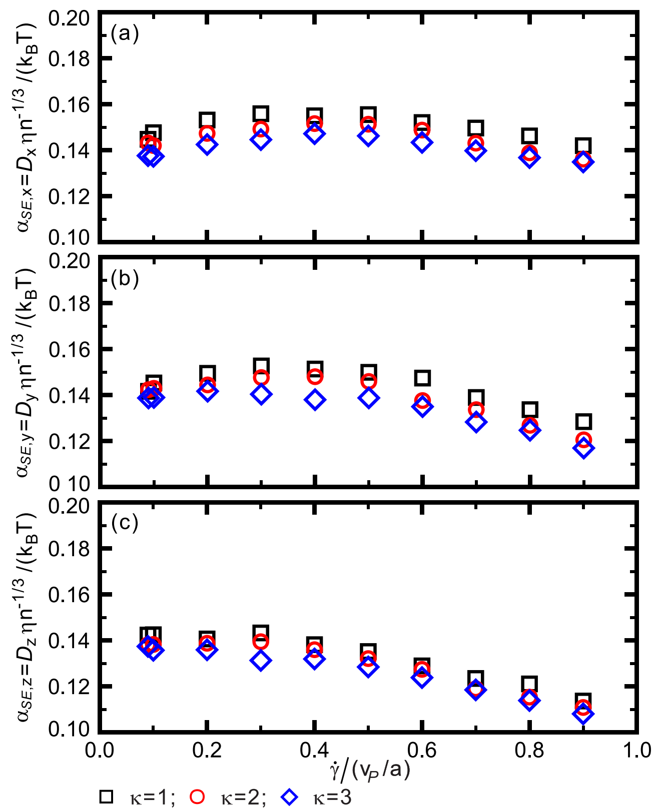

FIG. 7. Obtained reduced directional SE coefficients $\alpha_{{\rm SE},\beta}$ for 3D Yukawa fluids under steady shear in the flow direction [panel (a)], the velocity-gradient direction [panel (b)], and the vorticity direction [panel (c)], for $\kappa = 1$, 2, and 3, respectively. Here, the data of shear viscosity η and diffusion coefficient D are from Figs. 5 and 6, respectively. Clearly, under the lower shear rates, the calculated $\alpha_{{\rm SE},\beta}$ values for all directions and κ values are always $\approx$0.14, agreeing with the derived value of $\approx$0.132 for dense liquids in equilibrium. As the reduced shear rate $\dot{\gamma}/(\bar{v}_p/a)$ increases, the $\alpha_{{\rm SE},\beta}$ value in the velocity-gradient and vorticity directions decreases continuously, as shown in panels (b) and (c). However, the $\alpha_{{\rm SE},x}$ value does not change substantially with the shear rate, as shown in panel (a). Furthermore, under higher shear rates, the $\alpha_{{\rm SE},\beta}$ results exhibit both directional and κ dependence mainly due to the same property of the diffusion coefficient, indicating the breakdown of the SE relation at higher shear rates.

dynamics along the vorticity z direction, orthogonal to the x–y shear plane, does not directly participate in the macroscopic momentum transport. Consequently, the relatively weak enhancement of $\widetilde{D}_z$ in Fig. 6(c) fails to offset the global reduction of viscosity in Fig. 5, resulting in the most significant drop of the SE coefficient $\alpha_{\mathrm{SE},z}$. The velocity-gradient direction, which participates in the shear plane but measures transverse displacement rather than flow-directed momentum, exhibits an intermediate degree of compensation. In short, for our studied sheared 3D Yukawa liquidlike fluids, as a global measure, viscosity exhibits the isomorphic invariant; however, the diffusion exhibits different properties along three directions. Only along the shear direction, the SE relation is roughly obeyed, because viscosity and the diffusion along the x direction are both driven by the applied shear, probably suggesting that their mechanisms are coupled together. However, the diffusion along either the y or z direction is completely different from that along the x direction, so that the SE relation is violated.

V. SUMMARY

In summary, we perform NEMD simulations to study dynamics of 3D Yukawa liquidlike fluids under steady shears. Using simulation data, we calculate various physical quantities, such as the virial-potential-energy correlation, directional configurational temperature, RDF, shear viscosity, directional diffusion coefficient, and SE coefficient over a wide range of parameters. Our calculated Pearson correlation coefficient R value for sheared 3D Yukawa liquidlike fluids is always very close to unity, indicating possible isomorphic properties there.

We discover that, for our studied sheared 3D Yukawa liquidlike fluids, both the shear viscosity η and RDF $g(r)$ exhibit excellent isomorphic scaling properties, clearly indicated by the collapse of our calculated data points of either the η or $g(r)$ data points expressed in the isomorph reduced units for all studied κ values. The invariance of $g(r)$ means the averaged local configuration formed by neighboring particles is unchanged, although our studied 3D Yukawa fluids are continuously deformed and rearranged by the applied shear. We attribute the isomorphic scaling of shear viscosity to the dominant role of neighboring particles, whose configuration is unchanged as mentioned above. The isomorphic scaling of viscosity of sheared 3D Yukawa fluids exhibits the pronounced shear-thinning effect, which can be expressed as $\widetilde{\eta} = 2.13 - 0.956\widetilde{\gamma}^{*1/2}$ based on our data fitting.

We also calculate the diffusion coefficient of sheared 3D Yukawa fluids along different directions, where the contribution of the imposed shear is removed. We find that the diffusion is generally enhanced in all directions, while the directional anisotropy is also prominent. Along the flow direction, the enhancement of diffusion is the most significant, suggesting that the flow and peculiar velocities are somewhat linked together. The diffusion in the other two directions is less enhanced by the applied shear through the coupling of particle motion in 3D, from our understanding. Finally, we calculate the SE coefficient using the obtained viscosity and diffusion coefficient data. We find that the SE relation is roughly obeyed only along the flow direction; however, in the other two directions, the SE relation is violated. We attribute the breakdown of the SE relation to the increase of diffusion coefficient due to shear is not able to compensate for the substantial drop of shear viscosity from the shear-thinning effect.

ACKNOWLEDGMENTS

This work was supported by the National Key R&D Program of China under Grant No. 2025YFF0512000, the National Natural Science Foundation of China under Grant No. 12575214, the China Manned Space Program with Grant No. CMSS-2025-5-P-001, the 1000 Youth Talents Plan, and the Priority Academic Program Development (PAPD) of Jiangsu Higher Education Institutions.

DATA AVAILABILITY

There are no publicly available research data or software supporting this manuscript. Requests for further information or data should be sent to the authors.

[1] N. Gnan, T. B. Schrøder, U. R. Pedersen, N. P. Bailey, and J. C. Dyre, Pressure-energy correlations in liquids. IV. Isomorphs in liquid phase diagrams, J. Chem. Phys. **131**, 234504 (2009).

[2] J. C. Dyre, Isomorphs, hidden scale invariance, and quasiuniversality, Phys. Rev. E **88**, 042139 (2013).

[3] J. C. Dyre, Hidden scale invariance in condensed matter, J. Phys. Chem. B **118**, 10007 (2014).

[4] T. B. Schrøder and J. C. Dyre, Simplicity of condensed matter at its core: Generic definition of a Roskilde-simple system, J. Chem. Phys. **141**, 204502 (2014).

[5] U. R. Pedersen, N. P. Bailey, T. B. Schrøder, and J. C. Dyre, Strong pressure-energy correlations in van der Waals liquids, Phys. Rev. Lett. **100**, 015701 (2008).

[6] T. S. Ingebrigtsen, T. B. Schrøder, and J. C. Dyre, What is a simple liquid? Phys. Rev. X **2**, 011011 (2012).

[7] T. S. Ingebrigtsen, L. Bøhling, T. B. Schrøder, and J. C. Dyre, Communication: Thermodynamics of condensed matter with strong pressure-energy correlations, J. Chem. Phys. **136**, 061102 (2012).

[8] T. B. Schrøder, N. Gnan, U. R. Pedersen, N. P. Bailey, and J. C. Dyre, Pressure-energy correlations in liquids. V. Isomorphs in generalized Lennard-Jones systems, J. Chem. Phys. **134**, 164505 (2011).

[9] L. Bøhling, N. P. Bailey, T. B. Schrøder, and J. C. Dyre, Estimating the density-scaling exponent of a monatomic liquid from its pair potential, J. Chem. Phys. **140**, 124510 (2014).

[10] A. A. Veldhorst, T. B. Schrøder, and J. C. Dyre, Invariants in the Yukawa system's thermodynamic phase diagram, Phys. Plasmas **22**, 073705 (2015).

[11] F. Lucco Castello, P. Tolias, J. S. Hansen, and J. C. Dyre, Isomorph invariance and thermodynamics of repulsive dense bi-Yukawa one-component plasmas, Phys. Plasmas **26**, 053705 (2019).

[12] N. P. Bailey, U. R. Pedersen, N. Gnan, T. B. Schrøder, and J. C. Dyre, Pressure-energy correlations in liquids. I. Results from computer simulations, J. Chem. Phys. **129**, 184507 (2008).

[13] N. P. Bailey, U. R. Pedersen, N. Gnan, T. B. Schrøder, and J. C. Dyre, Pressure-energy correlations in liquids. II. Analysis and consequences, J. Chem. Phys. **129**, 184508 (2008).

[14] T. B. Schrøder, N. P. Bailey, U. R. Pedersen, N. Gnan, and J. C. Dyre, Pressure-energy correlations in liquids. III. Statistical mechanics and thermodynamics of liquids with hidden scale invariance, J. Chem. Phys. **131**, 234503 (2009).

[15] N. P. Bailey, L. Bøhling, A. A. Veldhorst, T. B. Schrøder, and J. C. Dyre, Statistical mechanics of Roskilde liquids: Configurational adiabats, specific heat contours, and density dependence of the scaling exponent, J. Chem. Phys. **139**, 184506 (2013).

[16] D. E. Albrechtsen, A. E. Olsen, U. R. Pedersen, T. B. Schrøder, and J. C. Dyre, Isomorph invariance of the structure and dynamics of classical crystals, Phys. Rev. B **90**, 094106 (2014).

[17] U. R. Pedersen, L. Costigliola, N. P. Bailey, T. B. Schrøder, and J. C. Dyre, Thermodynamics of freezing and melting, Nat. Commun. **7**, 12386 (2016).

[18] N. Yu, D. Huang, and Y. Feng, Melting curve of two-dimensional Yukawa systems predicted by isomorph theory, Phys. Rev. E **109**, 065212 (2024).

[19] Y. Rosenfeld, Relation between the transport coefficients and the internal entropy of simple systems, Phys. Rev. A **15**, 2545 (1977).

[20] Y. Rosenfeld, A quasi-universal scaling law for atomic transport in simple fluids, J. Phys.: Condens. Matter **11**, 5415 (1999).

[21] Y. Rosenfeld, Excess-entropy and freezing-temperature scalings for transport coefficients: Self-diffusion in Yukawa systems, Phys. Rev. E **62**, 7524 (2000).

[22] J.-P. Hansen and I. R. McDonald, *Theory of Simple Liquids: With Applications to Soft Matter* (Academic Press, Oxford, 2013), 4th ed.

[23] A. A. Veldhorst, J. C. Dyre, and T. B. Schrøder, Scaling of the dynamics of flexible Lennard-Jones chains, J. Chem. Phys. **141**, 054904 (2014).

[24] A. K. Bacher, T. B. Schrøder, and J. C. Dyre, Explaining why simple liquids are quasi-universal, Nat. Commun. **5**, 5424 (2014).

[25] L. Separdar, N. P. Bailey, T. B. Schrøder, S. Davatolhagh, and J. C. Dyre, Isomorph invariance of Couette shear flows simulated by the SLLOD equations of motion, J. Chem. Phys. **138**, 154505 (2013).

[26] J. C. Dyre, Isomorph theory beyond thermal equilibrium, J. Chem. Phys. **153**, 134502 (2020).

[27] S. Saw, L. Costigliola, and J. C. Dyre, Configurational temperature in active matter. I. Lines of invariant physics in the phase diagram of the Ornstein-Uhlenbeck model, Phys. Rev. E **107**, 024609 (2023).

[28] D. Jespersen, L. Costigliola, J. C. Dyre, and S. Saw, Active-matter isomorphs in the size-polydisperse Ornstein-Uhlenbeck Lennard-Jones model, J. Phys.: Condens. Matter **35**, 445101 (2023).

[29] D. J. Evans and G. P. Morriss, Non-Newtonian molecular dynamics, Comput. Phys. Rep. **1**, 297 (1984).

[30] D. J. Evans and G. P. Morriss, *Statistical Mechanics of Nonequilibrium Liquids* (Cambridge University Press, Cambridge, 2008).

[31] A. W. Lees and S. F. Edwards, The computer study of transport processes under extreme conditions, J. Phys. C: Solid State Phys. **5**, 1921 (1972).

[32] K. Miyazaki and D. R. Reichman, Molecular hydrodynamic theory of supercooled liquids and colloidal suspensions under shear, Phys. Rev. E **66**, 050501(R) (2002).

[33] V. Nosenko and J. Goree, Shear flows and shear viscosity in a two-dimensional Yukawa system (dusty plasma), Phys. Rev. Lett. **93**, 155004 (2004).

[34] Z. Donkó, J. Goree, P. Hartmann, and K. Kutasi, Shear viscosity and shear thinning in two-dimensional Yukawa liquids, Phys. Rev. Lett. **96**, 145003 (2006).

[35] Z. Donkó and P. Hartmann, Shear viscosity of strongly coupled Yukawa liquids, Phys. Rev. E **78**, 026408 (2008).

[36] Y. Feng, J. Goree, B. Liu, and E. G. D. Cohen, Green-Kubo relation for viscosity tested using experimental data for a two-dimensional dusty plasma, Phys. Rev. E **84**, 046412 (2011).

[37] D. Huang, S. Lu, and Y. Feng, Determination of viscosity in shear-induced melting two-dimensional dusty plasmas using Green-Kubo relation, Phys. Rev. E **103**, 013211 (2021).

[38] D. J. Searles and D. J. Evans, The fluctuation theorem and Green-Kubo relations, J. Chem. Phys. **112**, 9727 (2000).

[39] R. Zwanzig, On the relation between self-diffusion and viscosity of liquids, J. Chem. Phys. **79**, 4507 (1983).

[40] V. E. Fortov, A. V. Ivlev, S. A. Khrapak, A. G. Khrapak, and G. E. Morfill, Complex (dusty) plasmas: Current status, open issues, perspectives, Phys. Rep. **421**, 1 (2005).

[41] G. E. Morfill and A. V. Ivlev, Complex plasmas: An interdisciplinary research field, Rev. Mod. Phys. **81**, 1353 (2009).

[42] U. Konopka, G. E. Morfill, and L. Ratke, Measurement of the interaction potential of microspheres in the sheath of a rf discharge, Phys. Rev. Lett. **84**, 891 (2000).

[43] M. Bonitz, C. Henning, and D. Block, Complex plasmas: A laboratory for strong correlations, Rep. Prog. Phys. **73**, 066501 (2010).

[44] A. Melzer, *Physics of Dusty Plasmas* (Springer Nature, Cham, 2019).

[45] R. L. Merlino and J. A. Goree, Dusty plasmas in the laboratory, industry, and space, Phys. Today **57**(7), 32 (2004).

[46] J. Beckers, J. Berndt, D. Block, M. Bonitz, P. J. Bruggeman, L. Couëdel, G. L. Delzanno, Y. Feng, R. Gopalakrishnan, F. Greiner, *et al.*, Physics and applications of dusty plasmas: The perspectives 2023, Phys. Plasmas **30**, 120601 (2023).

[47] L. Couëdel, V. Nosenko, A. V. Ivlev, S. K. Zhdanov, H. M. Thomas, and G. E. Morfill, Direct observation of mode-coupling instability in two-dimensional plasma crystals, Phys. Rev. Lett. **104**, 195001 (2010).

[48] A. Mengel, F. X. Bronold, and F. Greiner, Evidence of different charging behavior of conductive and dielectric materials in low-temperature plasmas and a new diagnostic for low-energy electron absorption, Phys. Rev. Lett. **133**, 185301 (2024).

[49] C. A. Knapek, D. Samsonov, S. Zhdanov, U. Konopka, and G. E. Morfill, Recrystallization of a 2D plasma crystal, Phys. Rev. Lett. **98**, 015004 (2007).

[50] E. Thomas, Jr., J. D. Williams, and J. Silver, Application of stereoscopic particle image velocimetry to studies of transport in a dusty (complex) plasma, Phys. Plasmas **11**, L37 (2004).

[51] E. Thomas and J. Williams, Experimental measurements of velocity dissipation and neutral-drag effects during the formation of a dusty plasma, Phys. Rev. Lett. **95**, 055001 (2005).

[52] W. Yu, E. Abdelaleem, I. Nemenman, and J. C. Burton, Physics-tailored machine learning reveals unexpected physics in dusty plasmas, Proc. Natl. Acad. Sci. USA **122**, e2505725122 (2025).

[53] S. Hamaguchi, R. T. Farouki, and D. H. E. Dubin, Triple point of Yukawa systems, Phys. Rev. E **56**, 4671 (1997).

[54] S. Ichimaru, Strongly coupled plasmas: High-density classical plasmas and degenerate electron liquids, Rev. Mod. Phys. **54**, 1017 (1982).

[55] M. S. Murillo, Critical wave vectors for transverse modes in strongly coupled dusty plasmas, Phys. Rev. Lett. **85**, 2514 (2000).

[56] O. S. Vaulina and S. A. Khrapak, Scaling law for the fluid-solid phase transition in Yukawa systems (dusty plasmas), J. Exp. Theor. Phys. **90**, 287 (2000).

[57] O. Vaulina, S. Khrapak, and G. Morfill, Universal scaling in complex (dusty) plasmas, Phys. Rev. E **66**, 016404 (2002).

[58] S. A. Khrapak, Lindemann melting criterion in two dimensions, Phys. Rev. Res. **2**, 012040(R) (2020).

[59] J. H. Chu and L. I., Direct observation of Coulomb crystals and liquids in strongly coupled rf dusty plasmas, Phys. Rev. Lett. **72**, 4009 (1994).

[60] H. Thomas, G. E. Morfill, V. Demmel, J. Goree, B. Feuerbacher, and D. Möhlmann, Plasma crystal: Coulomb crystallization in a dusty plasma, Phys. Rev. Lett. **73**, 652 (1994).

[61] H. M. Thomas and G. E. Morfill, Melting dynamics of a plasma crystal, Nature (London) **379**, 806 (1996).

[62] L. I., W. T. Juan, C. H. Chiang, and J. H. Chu, Microscopic particle motions in strongly coupled dusty plasmas, Science **272**, 1626 (1996).

[63] A. Melzer, A. Homann, and A. Piel, Experimental investigation of the melting transition of the plasma crystal, Phys. Rev. E **53**, 2757 (1996).

[64] Y. Feng, J. Goree, and B. Liu, Solid superheating observed in two-dimensional strongly coupled dusty plasma, Phys. Rev. Lett. **100**, 205007 (2008).

[65] B. J. Harris, L. S. Matthews, and T. W. Hyde, Dusty plasma cavities: Probe-induced and natural, Phys. Rev. E **91**, 063105 (2015).

[66] C.-R. Du, V. Nosenko, H. M. Thomas, Y.-F. Lin, G. E. Morfill, and A. V. Ivlev, Slow dynamics in a quasi-two-dimensional binary complex plasma, Phys. Rev. Lett. **123**, 185002 (2019).

[67] Y.-F. He, B.-Q. Ai, C.-X. Dai, C. Song, R.-Q. Wang, W.-T. Sun, F.-C. Liu, and Y. Feng, Experimental demonstration of a dusty plasma ratchet rectification and its reversal, Phys. Rev. Lett. **124**, 075001 (2020).

[68] S. Singh, P. Bandyopadhyay, K. Kumar, and A. Sen, Square lattice formation in a monodisperse complex plasma, Phys. Rev. Lett. **129**, 115003 (2022).

[69] D. Huang, M. Baggioli, S. Lu, Z. Ma, and Y. Feng, Revealing the supercritical dynamics of dusty plasmas and their liquidlike to gaslike dynamical crossover, Phys. Rev. Res. **5**, 013149 (2023).

[70] M. Y. Pustylnik, B. Klumov, M. Rubin-Zuzic, A. M. Lipaev, V. Nosenko, D. Erdle, A. D. Usachev, A. V. Zobnin, V. I. Molotkov, G. Joyce, H. M. Thomas, M. H. Thoma, O. F. Petrov, V. E. Fortov, and O. Kononenko, Three-dimensional structure of a string-fluid complex plasma, Phys. Rev. Res. **2**, 033314 (2020).

[71] S. Mitic, M. Y. Pustylnik, D. Erdle, A. M. Lipaev, A. D. Usachev, A. V. Zobnin, M. H. Thoma, H. M. Thomas, O. F. Petrov, V. E. Fortov, and O. Kononenko, Long-term evolution of the three-dimensional structure of string-fluid complex plasmas in the PK-4 experiment, Phys. Rev. E **103**, 063212 (2021).

[72] V. Nosenko, M. Pustylnik, M. Rubin-Zuzic, A. M. Lipaev, A. V. Zobnin, A. D. Usachev, H. M. Thomas, M. H. Thoma, V. E. Fortov, O. Kononenko, and A. Ovchinin, Shear flow in a three-dimensional complex plasma in microgravity conditions, Phys. Rev. Res. **2**, 033404 (2020).

[73] Y. Feng, J. Goree, and B. Liu, Accurate particle position measurement from images, Rev. Sci. Instrum. **78**, 053704 (2007).

[74] Y. Feng, J. Goree, and B. Liu, Errors in particle tracking velocimetry with high-speed cameras, Rev. Sci. Instrum. **82**, 053707 (2011).

[75] A. Xu, N. Yu, D. Huang, and Y. Feng, Identifying liquidlike and gaslike states of dusty plasmas using isomorph theory, Phys. Rev. Res. **8**, 023016 (2026).

[76] N. Yu, D. Huang, S. Lu, S. Khrapak, and Y. Feng, Universal scaling of transverse sound speed and its isomorphic property in Yukawa fluids, Phys. Rev. E **109**, 035202 (2024).

[77] S. Khrapak, Stokes-Einstein relation in simple fluids revisited, Mol. Phys. **118**, e1643045 (2020).

[78] S. A. Khrapak and A. G. Khrapak, Excess entropy and Stokes-Einstein relation in simple fluids, Phys. Rev. E **104**, 044110 (2021).

[79] S. A. Khrapak, Self-diffusion in simple liquids as a random walk process, Molecules **26**, 7499 (2021).

[80] P. Xu, T. Cagin, and W. A. Goddard III, Assessment of phenomenological models for viscosity of liquids based on nonequilibrium atomistic simulations of copper, J. Chem. Phys. **123**, 104506 (2005).

[81] S. Plimpton, Fast parallel algorithms for short-range molecular dynamics, J. Comput. Phys. **117**, 1 (1995).

[82] H. Ohta and S. Hamaguchi, Molecular dynamics evaluation of self-diffusion in Yukawa systems, Phys. Plasmas **7**, 4506 (2000).

[83] K. Y. Sanbonmatsu and M. S. Murillo, Shear viscosity of strongly coupled Yukawa systems on finite length scales, Phys. Rev. Lett. **86**, 1215 (2001).

[84] T. Saigo and S. Hamaguchi, Shear viscosity of strongly coupled Yukawa systems, Phys. Plasmas **9**, 1210 (2002).

[85] H. H. Rugh, Dynamical approach to temperature, Phys. Rev. Lett. **78**, 772 (1997).

[86] B. D. Butler, G. Ayton, O. G. Jepps, and D. J. Evans, Configurational temperature: Verification of Monte Carlo simulations, J. Chem. Phys. **109**, 6519 (1998).

[87] J. Delhommelle and D. J. Evans, Configurational temperature thermostat for fluids undergoing shear flow: Application to liquid chlorine, Mol. Phys. **99**, 1825 (2001).

[88] F. Irgens, *Continuum Mechanics* (Springer, Berlin, 2008).

[89] G. E. Dieter, *Mechanical Metallurgy*, 3rd ed. (McGraw-Hill, New York, 1986).

[90] S. P. Timoshenko, *Strength of Materials, Part I: Elementary Theory and Problems*, 2nd ed. (D. Van Nostrand, New York, 1940).

[91] S. P. Timoshenko and J. N. Goodier, *Theory of Elasticity*, 2nd ed. (McGraw-Hill, New York, 1951).
[92] V. Nosenko, A. V. Ivlev, and G. E. Morfill, Microstructure of a liquid two-dimensional dusty plasma under shear, Phys. Rev. Lett. **108**, 135005 (2012).
[93] D. Huang, S. Lu, X.-Q. Shi, J. Goree, and Y. Feng, Fluctuation theorem convergence in a viscoelastic medium demonstrated experimentally using a dusty plasma, Phys. Rev. E **104**, 035207 (2021).
[94] H. J. M. Hanley, J. C. Rainwater, and S. Hess, Shear-induced angular dependence of the liquid pair correlation function, Phys. Rev. A **36**, 1795 (1987).
[95] D. Huang, S. Lu, M. S. Murillo, and Y. Feng, Origin of viscosity at individual particle level in Yukawa liquids, Phys. Rev. Res. **4**, 033064 (2022).
[96] D. Huang, S. Lu, C. Liang, M. Baggioli, and Y. Feng, Atomistic mechanisms of viscosity in 2D liquid-like fluids, Nat. Commun. **16**, 10171 (2025).
[97] S. A. Khrapak, Practical formula for the shear viscosity of Yukawa fluids, AIP Adv. **8**, 105226 (2018).
[98] K. Kawasaki and J. D. Gunton, Theory of nonlinear transport processes: Nonlinear shear viscosity and normal stress effects, Phys. Rev. A **8**, 2048 (1973).
[99] M. H. Ernst, B. Cichocki, J. R. Dorfman, J. Sharma, and H. van Beijeren, Kinetic theory of nonlinear viscous flow in two and three dimensions, J. Stat. Phys. **18**, 237 (1978).
[100] R. Zwanzig, Nonlinear shear viscosity and long time tails, Proc. Natl. Acad. Sci. USA **78**, 3296 (1981).
[101] V. Kumaran, Velocity autocorrelations and viscosity renormalization in sheared granular flows, Phys. Rev. Lett. **96**, 258002 (2006).
[102] L. Costigliola, D. M. Heyes, T. B. Schrøder, and J. C. Dyre, Revisiting the Stokes-Einstein relation without a hydrodynamic diameter, J. Chem. Phys. **150**, 021101 (2019).
[103] A. Einstein, Über die von der molekularkinetischen Theorie der Wärme geforderte Bewegung von in ruhenden Flüssigkeiten suspendierten Teilchen, Ann. Phys. **322**, 549 (1905).
[104] B. Liu, J. Goree, and O. S. Vaulina, Test of the Stokes-Einstein relation in a two-dimensional Yukawa liquid, Phys. Rev. Lett. **96**, 015005 (2006).